Published in final edited form as:
Psychiatry Res. 2014 November 30; 224(2): 73–80. doi:10.1016/j.pscychresns.2014.08.009.

Multimodal MRI markers support a model of small vessel ischemia for depressive symptoms in very old adults

Dana L. Tudorascu[a,b,e,*], **Caterina Rosano**[c], **Vijay K Venkatraman**[d], **Rebecca L MacCloud**[e], **Tamara Harris**[f], **Kristine Yaffe**[g], **Anne B Newman**[c], and **Howard J Aizenstein**[h,e,i]

[a]Department of Internal Medicine, University of Pittsburgh, Pittsburgh, PA, USA

[b]Department of Biostatistics, University of Pittsburgh, Pittsburgh, PA, USA

[c]Center for Aging and Population Health, Graduate School of Public Health, University of Pittsburgh, Pittsburgh, PA, USA

[d]Department of Neurosciences, School of Medicine, University of California, San Diego, CA, USA

[e]Geriatric Psychiatric Neuroimaging, Western Psychiatric Institute and Clinic, University of Pittsburgh, Pittsburgh, PA, USA

[f]Laboratory of Epidemiology, Demography, and Biometry, National Institute of Health, Bethesda, MD, USA

[g]Department of Psychiatry, Neurology and Epidemiology and Biostatistics, University of California, San Francisco, CA, USA

[h]Department of Bioengineering, University of Pittsburgh, Pittsburgh, PA, USA

[i]Department of Psychiatry, University of Pittsburgh, Pittsburgh, PA, USA

Abstract

In older adults, depressive symptoms are associated with lower quality of life, high morbidity and mortality. This study aims to identify brain magnetic resonance imaging (MRI) features associated with late-life depressive symptoms in the population. Older community-dwelling adults (n = 314) from the Health ABC study underwent brain MRI. Logistic regression was used to characterize the relationships between depressive symptoms (Center for Epidemiologic Studies of Depression scale, CES-D) and the following whole-brain variables: white matter hyperintensity (WMH) burden, fractional anisotropy (FA), and gray matter volume (GMV). Analyses examining possible regional differences between the CES-D groups controlled for Modified Mini-Mental State

[*]Corresponding author: tudorascudl@upmc.edu.

Institute of origin: Studies were carried out in the Geriatric Psychiatric Neuroimaging Section, Western Psychiatric Institute and Clinic, School of Medicine, University of Pittsburgh, Pittsburgh, PA.

Disclosure statement: Dana L. Tudorascu, Caterina Rosano, Vijay K Venkatraman, Rebecca L MacCloud, Tamara Harris, Kistine Yaffe, Anne B Newman, and Howard J Aizenstein do not have any potential conflict of interest to acknowledge.

Examination score and diabetes status. The relative importance of localization of the markers was examined by comparing the distribution of significant peaks across the brain. Each whole-brain variable showed loss of integrity associated with high CES-D. For GMV, the odds ratio (OR)=0.84 (95% confidence interval (CI) 0.74, 0.96); for FA, OR=0.714 (95% CI 0.57, 0.88); for WMH, OR=1.89 (95%CI 1.33, 2.69). Voxel-wise analyses and patterns of peak significance showed non-specific patterns for white matter measures. Loss of GMV was most significant in the bilateral insula and anterior cingulate cortex. This study supports a cerebrovascular pattern for depressive symptoms in older adults. The localization of gray matter changes to the insula, a watershed area and a hub of affective circuits, suggests an etiological pathway from ischemia to increased depressive burden.

Keywords

MRI markers; Depression; Geriatric

1. Introduction

Depressive symptoms in the elderly, which are common and associated with increased morbidity, have been identified as one of the leading causes of decreased quality of life in older individuals (Blazer, 2003). Brain-imaging correlates of these depressive symptoms would be helpful in understanding the biological mechanisms of depressive symptoms later in life, including major depression (often referred to in older adults as late-life depression, LLD). Magnetic resonance imaging (MRI) markers of brain integrity, including measures of gray matter volume, white matter lesion load, and myelin integrity, have all been associated with LLD (Bell-McGinty et al., 2002; Ballmaier and Toga, 2004; Wu et al., 2006; Andreescu et al., 2008; Sheline and Price, 2008; Butters and Aizenstein, 2009; Shimony et al., 2009). However, uncertainty remains about the primary pattern(s) of changes, and their causal implications, if any, for LLD. Is LLD due to damage from cerebrovascular insults, as posited by the vascular depression hypothesis (Alexopoulos and Meyers, 1997)? Does the pattern represent ‘toxic stress’ (Sheline and Wang, 1996) from cumulative lifetime depression burden? Or is depression part of the Alzheimer’s disease prodrome (Steffens and Plassman, 1997)? Studies support each of these models, and a single pattern has not emerged. Likely the failure to find definitive answers reflects the fact that LLD is itself heterogeneous and contains multiple patterns.

However, LLD is not necessarily the best model for studying depressive symptoms in the elderly. Several studies suggest that meeting full criteria for a major depressive episode is less common in older individuals than it is mid-life. Rather, it is the subsyndromal depressive symptom burden that appears to be more characteristic in the elderly (Lyness et al., 1999). Subsyndromal depression can be readily studied with epidemiological sampling methods. It may be that subsyndromal (or minor) depression in older adults represents a distinct disorder, related to major depressive disorder (MDD), but also similar to other geriatric syndromes(Lavretsky and Kumar, 2002). The current study aims to identify whether there is a pattern of structural and microstructural changes associated with

subsyndromal depressive symptoms that may point to a predominant pathway, with potential prevention and treatment targets.

The current study of 314 participants from the Health, Aging and Body Composition (Health ABC) Study uses multiple MRI sequences to quantify brain abnormalities at the macro-structural and micro-structural level including T1-weighted imaging, T2-weighted fluid-attenuated inversion recovery (FLAIR) imaging and diffusion tensor imaging (DTI). An aim of the study, which is based on a large epidemiologic sample, is to characterize the brain-imaging variables that are independently associated with depressive symptoms.

It has long been recognized that in the depressive symptoms in the elderly are often associated with cognitive deficits (Sheline et al., 2006). Thus, in studying brain-imaging variables associated with depressive symptoms, it is important to relate these changes to the individual's cognitive performance; otherwise, the brain changes found to be associated with depression might be primarily indicators of cognitive decline. We also included global cognitive performance, an additional independent variable, to distinguish the extent to which brain changes are primarily associated with the mood (and not cognitive) symptoms.

In this report, we examine the relationship of relevant MRI variables to depressive symptoms. In addition to examining the association of whole-brain markers of brain integrity, we also examine the regional distribution within the brain of these associations, using voxel-wise analyses. Further, to explore the relative regional specificity of these brain markers, we generate plots of the peak regional significance across the whole brain. This technique is used to visualize whether the markers show relatively similar effects across brain, or whether the plot shows distinct peaks, indicative of regional specificity.

2. Methods

2.1. Participants

Participants were recruited from the Pittsburgh Field Center of the Health ABC Study, an ongoing, longitudinal epidemiologic cohort study of well-functioning older men and women who were aged 70–79 at enrollment in 1997–1998. The Health ABC study was designed to determine the relationship of changes in body composition, weight, and related health conditions with incident mobility disability. In 2006–07, 325 Health ABC participants who were interested and eligible for a brain 3-Tesla MRI scan, and who were able to walk 20 m, participated in the Healthy Brain Project ancillary study at the Pittsburgh site. Of the 314 participants who were eligible for a 3-Tesla brain MRI, a total of 276 had complete MRI datasets, with measurements for all of the variables of interest. The University of Pittsburgh Institutional Review Board approved the protocol. All participants provided written informed consent.

2.2. Depressive symptom ratings

The Center for Epidemiologic Studies of Depression (CES-D) scale (Radloff, 1977) was used to measure depressive symptom burden in this population. Clinical diagnosis of depressive episodes or treatment for depression was not used. Instead this study focused on the relationship between the depressive symptom burden and MRI markers in the

community sample. The CES-D was dichotomized into low (CED-D<=10) and high (CES-D>10) scores to address non-normality of the distribution (visually examined using histograms and normal probability plots). A cut-off of 16 on the CES-D is often used to screen for clinically significant depressive symptoms. In this study, since we were interested in overall depressive symptom burden, we chose a lower threshold that has been supported by studies showing that significant depressive symptoms, as well one-fifth of depressive diagnoses, are missed with a cut-off score of 16 (Fechner-Bates et al., 1994; Hybels et al., 2001; Tamaria et al., 2013).

2.3. Image acquisition

MRI scanning was performed at the MR Research Center of the University of Pittsburgh. A 3-Tesla Siemens Tim Trio MR scanner was used, with a Siemens 12-channel head coil. Three series of MR images were analyzed for the current study, all acquired in the axial orientation as follows: *1. T1-weighted magnetization-prepared rapid gradient echo (MPRAGE)*, TR (repetition time) = 2300 ms, TE (echo time) =3.43 ms, inversion time (TI) = 900 ms, FA (flip angle) = 9 deg, slice thickness = 1 mm, FOV (field of view) = 256*224 mm, voxel size = 1 mm*1mm, and slices = 176; *2. T2-weighted fluid-attenuated inversion recovery (FLAIR)*, TR = 9160 ms, TE = 89 ms, TI = 2500 ms, FA = 150 deg, FOV = 256*212 mm, slice thickness=3 mm, slices=48, and voxel size= 1 mm*1 mm; *3. diffusion tensor imaging (DTI)*, single-short spin-echo sequence, TR = 5300 ms, TE = 88 ms, TI = 2500 ms, FA = 90 deg, FOV = 256*256 mm, two diffusion values of b=0 and 1000 s/mm, 12 diffusion directions, four repeats; 40 slices; voxel size= 2 mm*2 mm; slice thickness = 3mm, and GRAPPA (radial generalized auto-calibrating partially parallel acquisitions) =2.

2.4. Image processing

Global and regional markers of gray and white matter integrity were obtained using previously published methods (Venkatraman et al., 2011), briefly described below. Global brain tissue volumes (gray matter [GM], white matter [WM], and cerebrospinal fluid [CSF]) were estimated in cubic millimeters by segmenting the skull-stripped T1-weighted image using FAST – FMRIB's Automated Segmentation Tool (Zhang et al., 2001). Total intracranial volume (TICV) was calculated using BET (Smith, 2002) (Jenkinson et al., 2005), as the volume contained within the 'inner skull' segmentation. The gray matter volume marker was computed as a ratio between the total gray matter volume and total intracranial volume (TICV). The white matter hyperintensity (WMH) volume was obtained from the T2-weighted FLAIR image using an automated method for quantification and localization of WMH (Wu et al., 2006). The WMH quantification was done using a fuzzy connected algorithm. The total WMH volume was normalized for brain volume.

The diffusion-weighted images were pre-processed using the FMRIB's Diffusion Toolbox (Smith et al., 2004) to remove distortions due to eddy current, and the tensors were computed and diagonalized to determine the eigenvalues from which fractional anisotropy (FA) maps were computed (Pierpaoli and Basser, 1996). The FA map was registered to the FMRIB58_FA template (Smith et al., 2004) using FMRIB's Non-linear Image Registration Tool (FNIRT) (Andersson et al., 2007), similar to the Tract-based Spatial Statistics (TBSS) (Smith et al., 2006) program. Then, using the segmentations of WM, GM, and WMH that

were obtained from the magnetization prepared rapid gradient echo (MPRAGE) and T2-weighted FLAIR images, the FA map was restricted to normal appearing WM. Median FA was calculated for the normal appearing WM, throughout the brain, as well as in the white matter tracts identified in the Johns Hopkins White Matter Atlas (Wakana et al., 2004).

2.5. Statistical methods for whole-brain markers

The response variable, CES-D, was dichotomized into a binary variable (0 for a CES-D score ≤10, and 1 for a CES-D score >10). To test the relationship between CES-D scores and MRI variables, logistic regression models were used. The predictors of interest were gray matter volume (GMV), normalized mean FA, and WMH. The potential confounders were age, gender, score on the Modified Mini-Mental State Examination (3MSE, screening test that is used for dementia; Teng and Chui, 1987), cardiovascular disease, diabetes and hypertension. Cardiovascular disease, diabetes and hypertension were among the prevalent disease variables that were computed at the time of MRI using data collected since study entry in 1998–99. Coronary heart disease (CHD) was determined through self-report or Health Care Financing Administration (HCFA) data of myocardial infarction, angina, bypass or angioplasty. Determination of cardiovascular disease included self-reported CHD, cerebrovascular disease, or HCFA report of stroke. Stroke was determined through self-reported stroke, transient ischemia attack, or carotid endarterectomy. Diabetes mellitus status was determined through self-report, use of hypoglycemia medication, a fasting glucose of ≥126 mg/dl, or a 2-h glucose tolerance test >200 mg/dl, in accordance with the American Diabetes Association (ADA) criteria in 2002.

Differences in the confounders between the CES-D categories, CES-D ≤10 and CES-D >10, were tested and their statistical test values along with the corresponding *p*-values are presented in Table 1. For each CES-D category, means and standard deviations were computed (if the distribution was normal), as well as medians and interquartile range for non-normal variables and percentages for categorical and/or dichotomous variables. The two-sample *t*-test was used to test if there were any differences in the means of age between the two CES-D categories. Wilcoxon's rank sum was used to test differences in the distribution of the 3MSE between the two CES-D categories and chi-square tests for the association between gender and the CES-D categories, cardiovascular disease and CES-D, hypertension and CES-D, and diabetes and CES-D.

To compare the logistic regression models with different predictors, we have used the Deviance (G2) criteria (Agresti, 2007). Deviance is a quality of model fit statistic that compares two nested models. The addition of a variable to a model is tested using the Deviance criterion whose value is compared to a chi-square distribution (df=1). The criterion for significance would be to retain that variable in the model if the Deviance value is >3.84 = $\chi 2$ (1, 0.05).

2.6. Image-wise statistical analysis

Individual subject WMH, FA, and GM voxel-wise maps were used to explore the spatial distribution of the same markers examined in aggregate above. The methods used to generate voxel-wise maps of each marker are described below for each marker. In each case

we used the standard FSL (Smith et al., 2004) pre-processing stream, as well as FSL's Randomise for the second-level (i.e., group) comparisons of the individual subject contrast maps. Subjects were split into two groups: subjects with low CES-D (≤10) and with high CES-D (>10). Multiple regression models were constructed with the predictor of interest being CES-D group (low, high) and were adjusted for 3MSE and diabetes status. Statistical significance was determined using permutation-based non-parametric testing, with 5000 permutations, and threshold-free cluster enhancement (Smith and Nichols, 2009) to generate family-wise error (FWE) corrected statistical maps, with alpha set to less than 0.05.

2.6.1. Voxel-wise WMH prevalence—White matter hyperintensity maps were segmented from each individual's T2-weighted FLAIR image. These segmented maps were all transformed to common space by aligning each individual subject's FLAIR image to their DTI image (the non-diffusion B0 image) and aligned across subjects using FNIRT (Andersson et al., 2007). These WMH maps were then compared between the two CES_D groups using a multiple linear regression model that was adjusted for 3MSE and diabetes status.

2.6.2. Fractional anisotropy—Tract Based Spatial Statistics (TBSS) was performed using the FSL pipeline (Smith et al., 2006). This results in the creation of a mean FA image for each subject in common skeleton space. These individual subject FA-skeleton maps are used as the contrast maps to compare the two CES-D groups via multiple regression models adjusted for 3MSE and diabetes status.

2.6.3. Gray matter volume—Gray matter volume (GMV) was analyzed with FSL-VBM (Douaud et al., 2007; http://fsl.fmrib.ox.ac.uk/fsl/fslwiki/FSLVBM) using FSL tools (Smith et al., 2004). T1-weighted images were gray matter-segmented before being aligned to Montreal Neurological Institute (MNI) 152 standard space using non-linear registration (Andersson et al., 2007) and averaged to create a study-specific template. All native GM images were then non-linearly registered to this study-specific template, modulated, and smoothed. Voxel-based morphometry (VBM) was performed using these images as outcome measures, to evaluate the association between the GM density and CES-D groups while adjusting for 3MSE and diabetes status.

2.6.4. Regional distribution of whole brain changes for each marker—In addition to the probability maps showing significant differences between the groups for each marker, we also present plots of the *T*-statistics values for each region for each brain marker along with the total percentage of the voxels that made up the significant findings as the percentage of significance for the whole brain (Fig. 2 (GMV, 1.78%), Fig. 3 (upper) (FA, 48.19%), Fig.3 (lower) (WMH, 45.25%)). These plots display the differences between the groups in terms of *T*-maps. Each plot was generated by computing the total amount of gray matter volume (for VBM), white matter hyperintensities (for WMH) and FA skeleton (for FA) that was significant in the whole brain and the percentage corresponding to it. Then, for each region, the displayed *T*-statistic was computed as the average of highest *T*-statistics values corresponding to that specific percentage for each brain region.

3. Results

3.1. Description of the sample

The demographics and primary study measures for the sample are shown in Table 1 for each CES-D category. No significant differences were found between the two CES-D categories with respect to age (t=−1.22, df=275, p=0.225), cardiovascular disease (chi-square=2.86, df=1, p=0.568), hypertension (chi-square=1.25, df=1, p=0.263) or sex (chi-square=2.86, df=1, p=0.09). However, significant differences were found between the two CES-D groups with respect to the 3MSE variable (W=5307, p=0.025) and diabetes status (chi-square=5.01, df=1, p=0.025). The overall mean of the CES-S was 6.96 with a standard deviation of 6.29. The subjects in the low category had a CES-D mean of 4.23 with a standard deviation of 2.92 and in the high category had a much higher mean for CES-D of 16.23 and a standard deviation of 5.81.

3.2. Association of full brain neuroimaging markers with CES-D

A logistic regression model was used to examine the association between the CES-D and each brain marker. We first performed univariate logistic model analyses to look at the crude association between CES-D and each marker, and then the models were adjusted for 3MSE and diabetes status since statistically significant differences were detected between the two CES-D categories with respect to these variables. In addition, the chi-square value for testing the association between low and high CES-D and males and females had a p-value equal to 0.09; thus, we tested the addition of gender in the multiple logistic regression models as well.

3.3. Global gray matter volume

In the univariate logistic model, with only gray matter volume as a predictor, a significant relationship was found with the CES-D (p-value=0.012). The odds ratio (OR) of a CES-D of 10 or above is 0.84 for each unit (unit represents 1%) increase in the gray matter volume burden with a 95% confidence interval (CI) equal to 0.74, 0.96. Higher gray matter volume is less likely to be seen when the CES-D score is 10 or above.

Gray matter volume remained a significant predictor of the CES-D (OR=0.85, 95% CI (0.74, 0.97), p=0.023) when models were adjusted for gender, diabetes status and 3MSE. Also, all these variables were significantly associated with the CES-D (Table 2). For each one-unit increase in the gray matter volume, the odds of a CES-D score >10 decrease by 15% when diabetes status, gender and 3MSE are kept constant. Higher gray matter volume is less likely to be seen with a CES-D score >10.

When the model fit and residuals were examined, two subjects were detected with very large outlier values (Pearson chi-square >10, Deviance >4, Hosmer-Lemeshow goodness of fit p-value 0.07) causing instability in model estimation of parameters and a poor model fit. These outliers were removed from our model. The results that we present exclude those two subjects for this marker only.

3.4. Global white matter hyperintensity burden

A significant relationship was found between the WMH burden and CES-D categories (*p*-value=0). The odds ratio of a CES-D of 10 or above is 1.89 for each unit increase (1%) in the WMH burden with a 95% confidence interval equal to (1.33, 2.69). Higher WMH burden is more likely to be seen when CES-D is 10 or above.

When 3MSE and diabetes status are added to the model, WMH still remains significant (OR=1.87, 95% CI (1.30, 2.71), *p*=0), but neither 3MSE (*p*-value=0.233, 95% CI (0.50, 1.18)) nor diabetes status (*p*=0.07, 95% CI (0.95, 3.37)) is statistically significant (Table 2). The addition of gender was not statistically significant (chi-square equal to 2.84 with a *p*-value of 0.09); therefore, gender was removed from the model.

This shows that WMH are most prevalent in individuals with higher CES-D scores (greater than 10), independent of global cognitive performance, as measured by 3MSE and diabetes status. This suggests that these changes are unlikely to be secondary to an underlying, or prodromal, cognitive disorder.

3.5. Global white matter fractional anisotropy (FA)

Similarly as for the other markers, FA in normal appearing white matter (WM) in association with CES-D was examined using a univariate logistic model that was then adjusted for diabetes status and 3MSE. Gender was not significant in this model; thus, it was removed (differences in models with and without gender had a chi-square value of 1.86 with a *p*-value=0.17).

The associated unadjusted odds ratio for a one-unit (unit represents 1%) increase in FA in normal appearing white matter was 0.71 with a 95% confidence interval equal to (0.57, 0.88), *p*=0.002. When models were adjusted for diabetes status and 3MSE, the adjusted OR of having a CES-D score greater than 10 was 0.74 with a 95% CI equal to (0.60, 0.92) and a *p*-value of 0.008. None of the other variables were statistically significant (Table 2).

Thus, for each one-unit increase in the FA, the odds of a CES-D score >10 decrease by 26% when 3MSE and diabetes mellitus are kept constant. Higher overall WM FA is less likely to be seen when the CES-D score is high, 10 or above. Accordingly, there is a higher prevalence of individuals with low WM FA among those with higher CES-D scores, and this finding is independent of global cognitive performance; the same pattern of results is found for WMH, a macro-structural marker of ischemic changes. The microstructural WM FA measure is only for ‘normal appearing’ white matter, and therefore this measure excludes the WMH lesions. Thus, the observation that the same pattern holds for WM FA shows that WM alterations even outside of the macro-structural lesions are associated with depressive symptoms.

3.6. Voxel-wise association of neuroimaging markers with CES-D

In addition to examining the relationship of full-brain summary markers of white and gray matter integrity, voxel-wise analyses were also performed to identify the regional patterns of white and gray matter changes with depressive symptoms. As with the logistic regression

analyses for the whole-brain measures, each of these maps (corrected for multiple comparisons, with family-wise error) shows significant differences between the groups; similarly, the effects are in the expected direction – loss of integrity in the markers is most pronounced in the group with high CES-D scores. These voxel-wise results for WMH, FA, and gray matter volume are described below.

3.7. Regional pattern of FA association with CES-D

Fig. 1 shows the significance maps of FA multiple regression for the association between the FA and CES-D groups while controlling for 3MSE and diabetes status. The statistical map, overlaid on the mean FA skeleton, is shown in Fig. 1. There are extensive regions of significance throughout the white matter. Consistent with previous findings in LLD (Taylor et al., 2008), the FA is associated with depressive symptoms in the anterior cingulum. However, the FA changes are not localized only to the anterior cingulum, but appear in a diffuse pattern throughout the skeleton.

3.8. Regional pattern of gray matter volume association with CES-D

Results of the VBM analysis of the gray matter volume changes associated with CES-D are shown in Fig. 1. The most significant differences identified in this map are in the anterior cingulate and left insula (both anterior and posterior aspects), as well as in the volume loss in the insula and the right transverse temporal gyrus. The insula is both a prominent watershed area in the brain, particularly susceptible to low-perfusion ischemia, and also a prominent region in the mood circuits (Sprengelmeyer et al., 2011).

3.9. Regional pattern of WMH association with CES-D

The relationships of the WMH and CES-D groups that were evaluated using multiple regression models adjusted for 3MSE and diabetes status are displayed as a statistical map in Fig. 1, thresholded with a family-wise-error threshold of $p<0.05$. As expected, the high CES-D group had a significantly higher burden of WMH in those white matter regions where WMH are generally seen, primarily in the periventricular regions. Whereas in individual subject WMH maps small clusters of deep white matter are also found, it is not surprising that these are not as apparent in the group map, since the regions are small and may not have enough spatial overlap across subjects to be evident in the group analysis.

No other statistically significant areas that survived the FWE correction were present on any of the maps (FA, GMV or WMH).

3.10. Regional distribution of whole-brain changes for each marker

The whole brain marker analyses (described in Sections 3.2–3.5) show that each of the markers is associated with depressive symptoms, and the maps show where the peaks are. One limitation in viewing these statistical maps is that it is not clear whether the peaks are indicative of a true regional specificity, or perhaps an artifact of the chosen statistical threshold used for visualizing the statistical map. That is, the apparent localization map, may reflect only small statistical differences from other regions, whereas in fact since systemic factors are associated with changes in these brain markers, the whole brain is similarly effected. To address this distinction between regional and global significance, we generated

individual marker plots of the maximum *T*-values across the gray and white matter regions for the three markers of interest: Fig. 2 (distribution of gray matter volume), Fig. 3 (upper) (distribution of FA), and Fig. 3 (lower) (distribution of WMH). As expected, the peaks in these plots are the same regions identified in the voxel-based analyses (described in Sections 3.6–3.8), e.g., the anterior cingulate and left insula are seen as peaks in the GMV plot (Fig. 2). These plots support the view of regional specificity for GMV measures: there appear to be distinct peaks for the GMV, with maximum *T*-value sranging from o.3 in the globus pallidum to 4.5 in the right anterior cingulate. For the FA and WMH plots, the pattern appears less supportive of regional specificity. For the FA plots, the mean FA ranges from 1.22 in the cingulum and left hippocampus to 3.0 for the Forceps minor (FSL JHU white matter JHU white-matter tractography atlas, 20 structures)(Wakana et al., 2004; Mori et al., 2005). Similarly, the plot of regional specificity for WMH burden is also relatively flat, with all but one region in the range of 1.6 to 3.2.

4. Discussion

The aim of this study was to investigate the association of brain-imaging measures and late-life depressive symptoms. Our results reveal statistically significant relationships between each class of markers and CES-D score; in each case, loss of integrity of the whole brain markers (higher WMH burden, lower WM FA, and lower global gray matter volume), was most likely in the high CES-D group (CES-D score >10). Thus, as has been shown in clinical samples of patients with major depression, each of these markers was significantly associated with depressive symptom burden in a large community sample.

A strength of this study was that the sample size and available ancillary measures also allowed for the evaluation of whether global cognitive performance (as measured by 3MSE) influenced the relationship between the imaging markers and the depressive symptoms. As expected, 3MSE was significantly associated with depressive symptoms; however, for each marker the relationship between the global imaging marker and CES-D group remained significant even when 3MSE was included in the model. Thus, we have demonstrated that, even though cognitive impairment and depressive symptoms are highly related, there remain structural brain changes in both gray and white matter that are independently associated with depressive symptoms.

The observation that WM FA and gray matter volume were not independently associated with depressive symptoms, even in this relatively large sample, raises the issue of whether these brain-imaging markers may be primarily related to depressive symptoms through shared factors also associated with WMH (e.g., cerebrovascular risk factors leading to loss of integrity in all markers). The results regarding the relative independence of these imaging markers only apply to the whole-brain measures; therefore, it is still possible that the regional distribution of WM FA and gray matter atrophy might be associated with CES-D score independent of WMH burden.

Localization of imaging markers was also examined. The regional distribution of WMH, WM FA, and GM volume were investigated relative to CES-D score, using multiple regression models adjusted for 3MSE and diabetes status. The regional distributions of these

markers showed diffuse patterns for the two white matter measures: FA changes were apparent throughout the white matter skeleton, including the anterior cingulate, and the areas of significant effects in the WMH contrast were around the ventricles, in the expected areas where there tend to be confluent WM lesions. The regional specificity of these imaging markers was further explored by looking at plots of peak *T*-values across the brain. These plots support a model that for GMV there is regional specificity of the association of these markers with CES-D, but for WMH and FA, the associations with the CES-D are relatively diffuse across the brain. This supports a previous report that regional WMH burden is highly associated with overall WMH burden (DeCarli et al., 2005).

The gray matter volume changes were most significant in the left insula and anterior cingulate, consistent with previous reports of a central role of the insula in mood disorders (Hamilton and Etkin, 2012); specifically, the anterior insula has been strongly associated with interpersonal appreciation (Wicker et al., 2003; Jabbi et al., 2008). The insula is also a major watershed area, particularly susceptible to hypo-perfusion states. It is possible that the primary vascular association, identified by the independence of global WMH burden, is also reflected by the localization of the GM changes to a watershed area. We speculate that common chronic hypoperfusion conditions in the older adults, including congestive heart failure and orthostatic hypotension, may lead to chronic non-specific white matter ischemia (WMH) and atrophy in the insula. Further, based on the known functions of insular circuits, we speculate that this damage leads to a deficit in social interpersonal awareness, and an apathetic depressive state.

We also note that both the anterior insula and the rostral anterior cingulate have been key regions associated with altered mood regulation and depressive disorders (e.g., Phillips). In particular the insula (primarily the anterior portion), which is a key hub in the salience network, and the rostral anterior, which has a central role in emotion regulation, are both considered part of the limbic circuit (Papez, 1995), long recognized as playing a key role in emotion.

The primary impact of this finding is its thorough characterization of the primary imaging correlates of depressive symptoms in a large epidemiological sample of community-dwelling older adults. We found that all three imaging markers are associated with depressive symptoms independent of general cognitive function. The prominence of WMH in the multivariate model and the regional pattern of lower gray matter volume in watershed areas both suggest an ischemic pattern. These results are qualified by the adequacy of measures of depressive symptoms and cognition. In both cases (CES-D and 3MSE), the measures are very coarse, with limited sensitivity. Future studies with finer measures of cognitive and mood domains can further clarify these initial findings.

We suspect that the vascular risk factors (in this case cardiovascular disease, diabetes and hypertension) are similar between groups, despite differences in WMH, due to the distinct contribution of a depressive syndrome on inflammatory and vascular pathways; the depressive syndrome thus contributes to WMH load independent of other identified vascular risk factors. The main clinical significance of this study its finding that in an epidemiological sample of older adults, even subsyndromal depressive symptoms are

associated with both gray matter and white matter alterations. Moreover, secondary analyses of the localization of these findings suggest that gray matter atrophy is localized to the insula and rostral anterior cingulate cortex, but the white matter alterations are somewhat non-specific, reflecting a systemic whole-brain effect. This suggests that future studies of white matter alterations in late-life depressive disorders may use whole-brain white matter markers, instead of diluting the statistical power of the analysis with a multitude of regional (or voxel-level) variables.

There are also several limitations in this study. Depressive symptoms are defined solely through the self-administered CES-D scale. Expert structured clinical interviews (such as the Structured Clinical Interview for DSM-IV (First et al., 1997)) are the gold standard for depression diagnoses. However, structured interviews were not obtained in this epidemiological study. The study is also limited in its approach for distinguishing the independent contributions of the different regional versus global imaging markers. We used a qualitative approach by examining the distribution of effect sizes across the brain. Future studies with more sophisticated quantitative comparisons of regional versus global markers would be necessary to more confidently address the relative contribution of regional versus global imaging markers.

Acknowledgments

This work was supported by the Healthy Brain and Resilience grant founded by the National Institutes of Health/ National Institutes of Aging, R01 AG29232-05, R01 AG037451-01 and National Institute of Mental Health R01 MH086498.

References

Expert Committee on the Diagnosis and Classification of Diabetes Mellitus. Report of the Expert Committee on the Diagnosis and Classification of Diabetes Mellitus. 2002:S5–20.

Agresti A. An introduction to categorical data analysis (2). 2007

Alexopoulos GS, Meyers BS. Vascular depression hypothesis. Archives of General Psychiatry. 1997; 54:915–922. [PubMed: 9337771]

Andersson JLR, Jenkinson M, Smith S. Non-linear registration aka Spatial normalisation FMRIB Technial Report TR07JA2. In Practice. 2007:22–22.

Andreescu C, Butters MA, Begley A, Rajji T, Wu MJ, Meltzer CC, Reynolds CF, Aizenstein H. Gray matter changes in late life depression – a structural MRI analysis. Neuropsychopharmacology. 2008; 33:2566–2572. [PubMed: 18075490]

Ballmaier M, Toga AW. Anterior cingulate, gyrus rectus, and orbitofrontal abnormalities in elderly depressed patients: an MRI-based parcellation of the prefrontal cortex. American Journal of Psychiatry. 2004; 161:99–108. [PubMed: 14702257]

Bell-McGinty S, Butters MA, Meltzer CC, Greer PJ, Reynolds CF, Becker JT. Brain morphometric abnormalities in geriatric depression: long-term neurobiological effects of illness duration. American Journal of Psychiatry. 2002; 159:1424–1427. [PubMed: 12153839]

Blazer DG. Depression in late life: review and commentary. The Journals of Gerontology Series A Biological Sciences and Medical Sciences. 2003; 58:M249–M265.

Butters MA, Aizenstein HJ. Three-dimensional surface mapping of the caudate nucleus in late-life depression. The American Journal of Geriatric Psychiatry. 2009; 17:4–12. [PubMed: 18790876]

DeCarli C, Fletcher E, Ramey V, Harvey D, Jagust WJ. Anatomical mapping of white matter hyperintensities (WMH): exploring the relationships between periventricular WMH, deep WMH, and total WMH burden. Stroke: A Journal of Cerebral circulation. 2005; 36:50–55. [PubMed: 15576652]

Douaud G, Smith S, Jenkinson M, Behrens T, Johansen-Berg H, Vickers J, James S, Voets N, Watkins K, Matthews PM, James A. Anatomically related grey and white matter abnormalities in adolescent-onset schizophrenia. Brain: A Journal of Neurology. 2007; 130:2375–2386. [PubMed: 17698497]

Fechner-Bates S, Coyne JC, Schwenk TL. The relationship of self-reported distress to depressive disorders and other psychopathology. Journal of Consulting and Clinical Psychology. 1994; 62:550–559. [PubMed: 8063981]

First, MB.; Spitzer, RL.; Gibbon, M.; Williams, JBW. Structured Clinical Interview for DSM-IV Axis I Disorders, Clinician Version (SCID-CV). American Psychiatric Association; Washington, DC: 1997.

Hamilton JP, Etkin A. Functional neuroimaging of major depressive disorder: a meta-analysis and new integration of baseline activation and neural response data. American Journal of Psychiatry. 2012; 169:693–703. [PubMed: 22535198]

Hua K, Zhang J, Wakana S, Jiang H, Li X, Reich DS, Calabresi PA, Pekar JJ, van Zijl PCM, Mori S. Tract probability maps in stereotaxic spaces: analyses of white matter anatomy and tract-specific quantification. NeuroImage. 2008; 39:336–347. [PubMed: 17931890]

Hybels CF, Blazer DG, Pieper CF. Toward a threshold for subthreshold depression: an analysis of correlates of depression by severity of symptoms using data from an elderly community sample. The Gerontologist. 2001; 41:357–365. [PubMed: 11405433]

Jabbi M, Bastiaansen J, Keysers C. A common anterior insula representation of disgust observation, experience and imagination shows divergent functional connectivity pathways. PloS One. 2008; 3:e2939–e2939. [PubMed: 18698355]

Jenkinson M, Pechaud M, Smith S. BET2: MR-based estimation of brain, skull and scalp surfaces. Eleventh annual meeting of the Organization for Human Brain Mapping. 2005

Lavretsky H, Kumar A. Clinically significant non-major depression: old concepts, new insights. The American Journal of Geriatric Psychiatry. 2002; 10:239–255. [PubMed: 11994211]

Lyness JM, King DA, Cox C. The importance of subsyndromal depression in older primary care patients: prevalence and associated functional disability. Journal of the American Geriatrics Society. 1999; 47:647–652. [PubMed: 10366161]

Mori, S.; Wakana, S.; Nagae-Poetscher, LM.; Van Zijl, PCM. MRI Atlas of Human White Matter. Elsevier; Amsterdam: 2005.

Papez JW. A proposed mechanism of emotion. 1937. The Journal of Neuropsychiatry and Clinical Neurosciences. 1995; 7:103–112. [PubMed: 7711480]

Pierpaoli C, Basser PJ. Toward a quantitative assessment of diffusion anisotropy. Magnetic Resonance in Medicine. 1996; 36:893–906. [PubMed: 8946355]

Radloff LS. The CES-D scale a self-report depression scale for research in the general population. Applied Psychological Measurement. 1977; 1:385–401.

Sheline Y, Price J. Regional white matter hyperintensity burden in automated segmentation distinguishes late-life depressed subjects from comparison subjects matched for vascular risk factors. American Journal of Psychiatry. 2008; 165:524–532. [PubMed: 18281408]

Sheline YI, Barch DM, Garcia K, Gersing K, Pieper C, Welsh-Bohmer K, Steffens DC, Doraiswamy PM. Cognitive function in late life depression: relationships to depression severity, cerebrovascular risk factors and processing speed. Biological Psychiatry. 2006; 60:58–65. [PubMed: 16414031]

Sheline YI, Wang PW. Hippocampal atrophy in recurrent major depression. Proceedings of the National Academy of Sciences of the United States of America. 1996; 93:3908–3913. [PubMed: 8632988]

Shimony J, Sheline Y, D'Angelo G. Diffuse microstructural abnormalities of normal-appearing white matter in late life depression: a diffusion tensor imaging study. Biological Psychiatry. 2009; 66:245–252. [PubMed: 19375071]

Smith SM. Fast robust automated brain extraction. Human Brain Mapping. 2002; 17:143–155. [PubMed: 12391568]

Smith SM, Jenkinson M, Johansen-Berg H. Tract-based spatial statistics: voxelwise analysis of multi-subject diffusion data. Neuroimage. 2006; 31:1487–1505. [PubMed: 16624579]

Smith SM, Jenkinson M, Woolrich MW. Advances in functional and structural MR image analysis and implementation as FSL. Neuroimage. 2004; 23:S208–S219. [PubMed: 15501092]

Smith SM, Nichols TE. Threshold-free cluster enhancement: addressing problems of smoothing, threshold dependence and localisation in cluster inference. NeuroImage. 2009; 44:83–98. [PubMed: 18501637]

Sprengelmeyer R, Steele JD, Mwangi B, Kumar P, Christmas D, Milders M, Matthews K. The insular cortex and the neuroanatomy of major depression. Journal of Affective Disorders. 2011; 133:120–127. [PubMed: 21531027]

Steffens DC, Plassman BL. A twin study of late-onset depression and apolipoprotein E ε4 as risk factors for Alzheimer's disease. Biological Psychiatry. 1997; 41:851–856. [PubMed: 9099411]

Tamaria A, Bharti R, Sharma M, Dewan R, Kapoor G, Aggarwal A, Batra A, Batra A. Risk assessment for psychological disorders in postmenopausal women. Journal of Clinical and Diagnostic Research. 2013; 7:2885–2888. [PubMed: 24551665]

Taylor WD, Kuchibhatla M, Payne ME. Frontal white matter anisotropy and antidepressant remission in late-life depression. PLoS One. 2008; 3:e3267–e3267. [PubMed: 18813343]

Teng EL, Chui HC. The Modified Mini-Mental State (3MS) examination. The Journal of Clinical Psychiatry. 1987; 48:314–318. [PubMed: 3611032]

Venkatraman VK, Aizenstein HJ, Newman AB, Yaffe K, Harris T, Kritchevsky S, Ayonayon HN, Rosano C. Lower digit symbol substitution score in the oldest old is related to magnetization transfer and diffusion tensor imaging of the white matter. Frontiers in Aging Neuroscience. 2011; 3:1–8. [PubMed: 21442044]

Wakana S, Jiang H, Nagae-Poetscher LM, Zijl PCMV, Mori S. Fiber tract–based atlas of human white matter anatomy1. Radiology. 2004; 230:77–87. [PubMed: 14645885]

Wicker B, Keysers C, Plailly J, Royet JP. Both of us disgusted in my insula: the common neural basis of seeing and feeling disgust. Neuron. 2003; 40:655–664. [PubMed: 14642287]

Wu M, Rosano C, Butters M, Whyte E, Nable M, Crooks R, Meltzer CC, Reynolds CF, Aizenstein HJ. A fully automated method for quantifying and localizing white matter hyperintensities on MR images. Psychiatry Research: Neuroimaging. 2006; 148:133–142.

Zhang Y, Brady M, Smith S. Segmentation of brain MR images through a hidden Markov random field model and the expectation-maximization algorithm. IEEE Transactions on Medical Imaging. 2001; 20:45–57. [PubMed: 11293691]

Tudorascu Highlights

- This study examined brain magnetic resonance imaging (MRI) features associated with late-life depressive symptoms in a community sample
- MRI variables examined were: white matter hyperintensity burden, fractional anisotropy and gray matter volume
- Each whole-brain variable showed loss of integrity associated with high higher depression score on the CES-D.
- Findings support a cerebrovascular pattern for depressive symptoms in older adults.

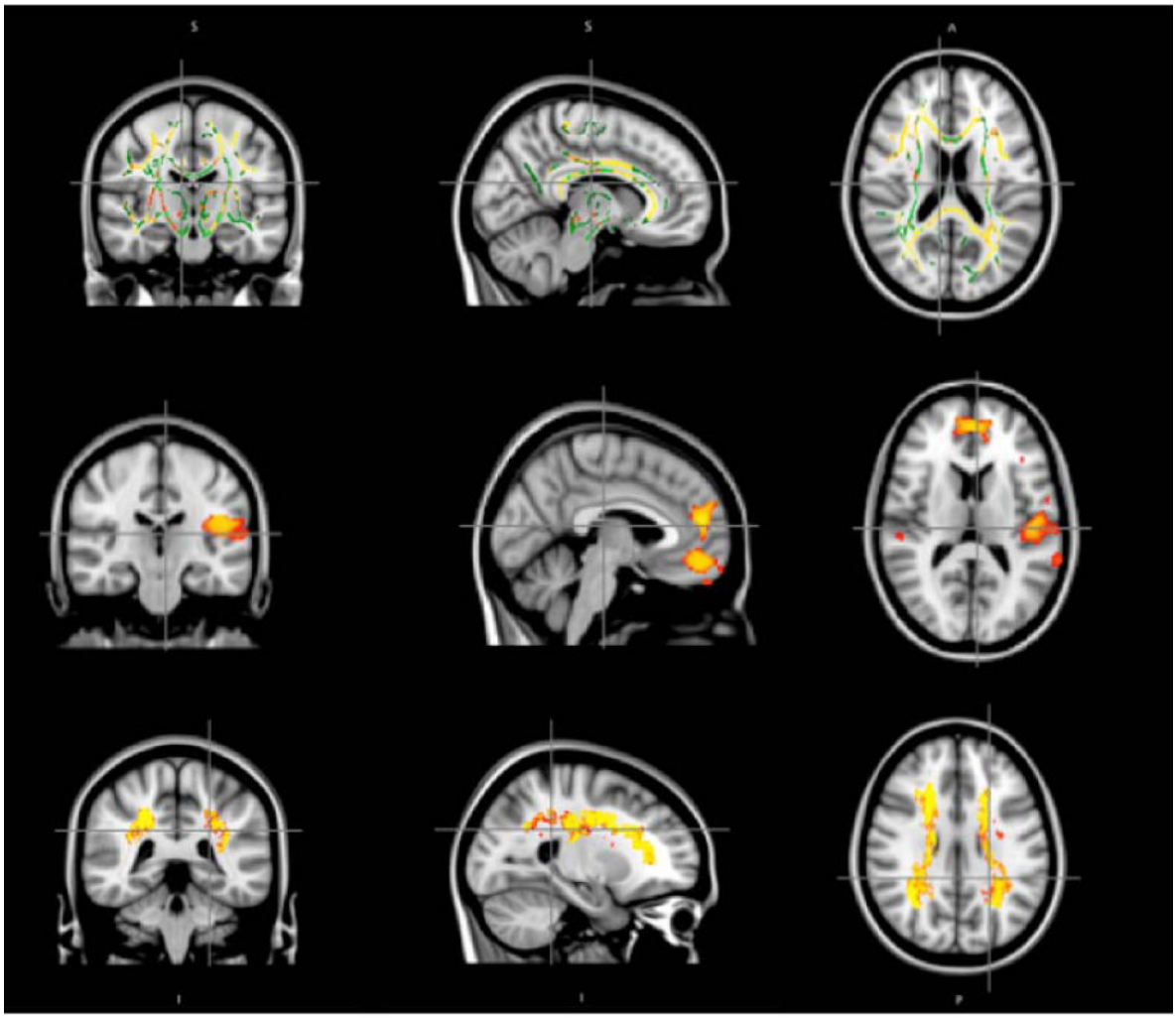

In order from top to bottom: FA map of comparison: Low CES-D>High CES-D, VBM map of comparison, Low CES-D>High CES-D, WMH map of comparison, High CES-D>Low CES-D. All maps are FWE corrected (p<.05).

Figure 1.
FA, GMV, WMH group comparison

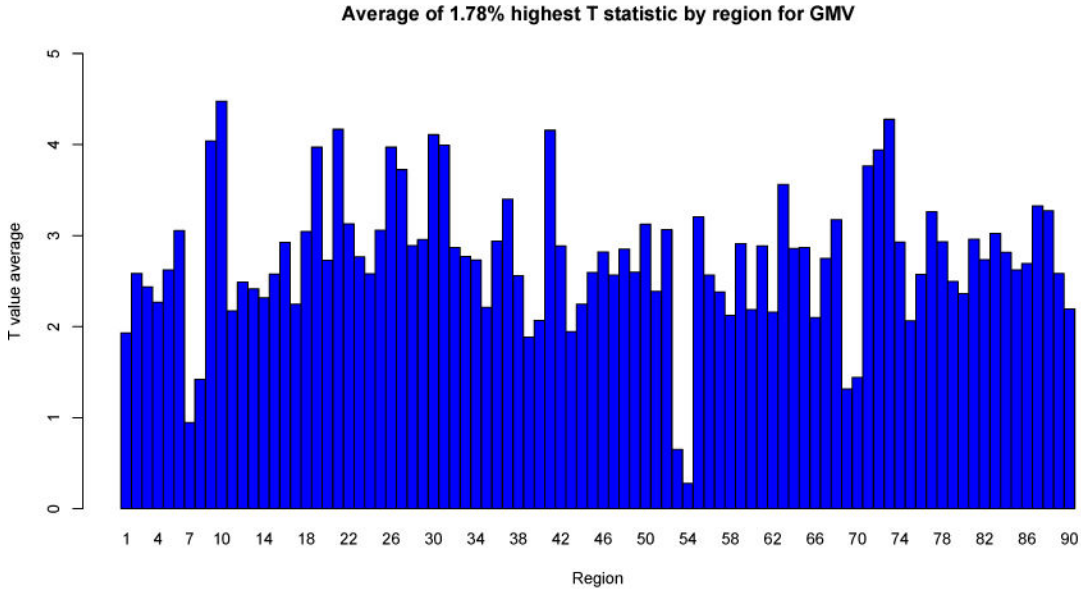

1 Amygdala_L
2 Amygdala_R
3 Angular_L
4 Angular_R
5 Calcarine_L
6 Calcarine_R
7 Caudate_L
8 Caudate_R
9 Cingulum_Ant_L
10 Cingulum_Ant_R
11 Cingulum_Mid_L
12 Cingulum_Mid_R
13 Cingulum_Post_L
14 Cingulum_Post_R
15 Cuneus_L
16 Cuneus_R
17 Frontal_Inf_Oper_L
18 Frontal_Inf_Oper_R
19 Frontal_Inf_Orb_L
20 Frontal_Inf_Orb_R
21 Frontal_Inf_Tri_L
22 Frontal_Inf_Tri_R
23 Frontal_Latx_Orb_L
24 Frontal_Latx_Orb_R
25 Frontal_Mid_L
26 Frontal_Mid_Orb_L
27 Frontal_Mid_Orb_R
28 Frontal_Mid_R
29 Frontal_Sup_L
30 Frontal_Sup_Medial_L
31 Frontal_Sup_Medial_R
32 Frontal_Sup_Orb_L
33 Frontal_Sup_Orb_R
34 Frontal_Sup_R
35 Fusiform_L
36 Fusiform_R
37 Heschl_L
38 Heschl_R
39 Hippocampus_L
40 Hippocampus_R
41 Insula_L
42 Insula_R
43 Lingual_L
44 Lingual_R
45 Occipital_Inf_L
46 Occipital_Inf_R
47 Occipital_Mid_L
48 Occipital_Mid_R
49 Occipital_Sup_L
50 Occipital_Sup_R
51 Olfactory_L
52 Olfactory_R
53 Pallidum_L
54 Pallidum_R
55 Paracentral_Lobule_L
56 Paracentral_Lobule_R
57 ParaHippocampal_L
58 ParaHippocampal_R
59 Parietal_Inf_L
60 Parietal_Inf_R_
61 Parietal_Sup_L
62 Parietal_Sup_R
63 Postcentral_L
64 Postcentral_R
65 Precentral_L
66 Precentral_R
67 Precuneus_L
68 Precuneus_R
69 Putamen_L
70 Putamen_R
71 Rectus_L
72 Rectus_R
73 Rolandic_Oper_L
74 Rolandic_Oper_R
75 Supp_Motor_Area_L
76 Supp_Motor_Area_R
77 SupraMarginal_L
78 SupraMarginal_R
79 Temporal_Inf_L
80 Temporal_Inf_R
81 Temporal_Mid_L
82 Temporal_Mid_R
83 Temporal_Pole_Mid_L
84 Temporal_Pole_Mid_R
85 Temporal_Pole_Sup_L
86 Temporal_Pole_Sup_R
87 Temporal_Sup_L
88 Temporal_Sup_R
89 Thalamus_L
90 Thalamus_R

Figure 2.
GMV plot

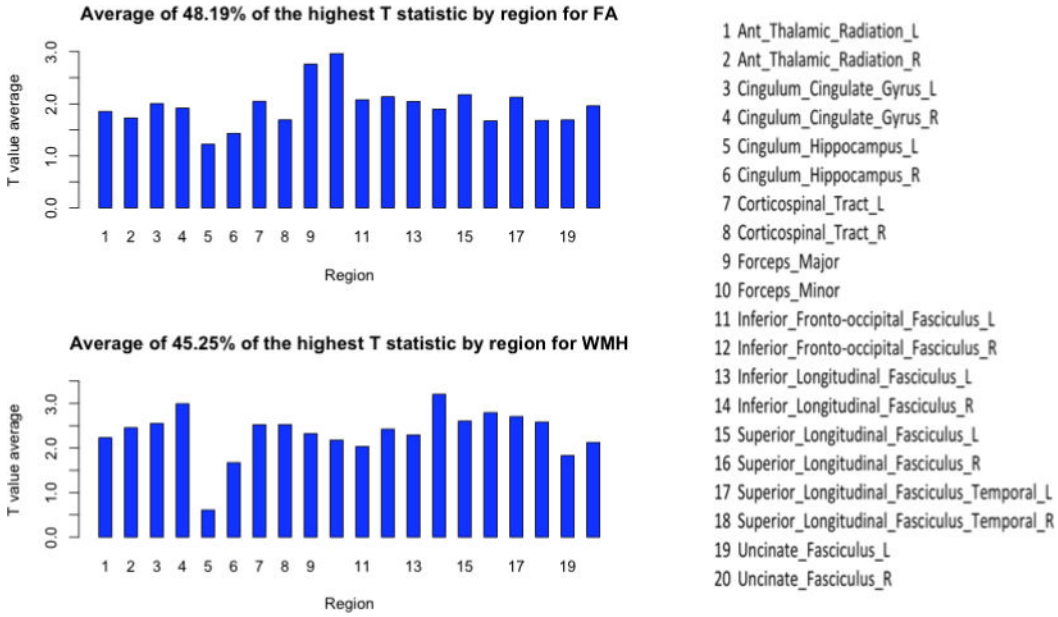

Figure 3.
FA and WMH plots

Table 1

Demographics and primary study measures by CES-D categories:

CES-D levels/variables	Low CES-D *N*=214		High CES-D *N*=63		*p*-value
Age	82.83[a]	2.57[b]	83.39[a]	3.26[b]	0.225
Sex (m, %)	97	45 %	21	33%	0.09
3MSE	95 [c]	7[d]	93[c]	12[d]	0.025
Cardiovascular disease (%)	60	28%	20	31.7%	0.568
Diabetes (%)	51	23.8%	24	38.1%	0.025
Hypertension (%)	173	81.2 %	55	87.3%	0.263

[a] mean

[b] standard deviation

[c] median

[d] interquartile range. All *p*-values are two tailed.

All *p*-values are two tailed.

Table 2

Multiple logistic regression results for CES-D with each brain marker:

Predictor	β	Se (β)	Wald	df	*p*	OR	95% CI for OR
Gray matter volume (GMV)							
GMV	−0.159	0.070	5.171	1	0.023	0.85	(0.74,0.97)
Diabetes	−0.768	0.328	5.462	1	0.019	0.46	(0.24,0.88)
Gender	−0.768	0.332	5.347	1	0.020	0.46	(0.24,0.89)
3MSE	−0.046	0.021	4.553	1	0.032	0.62	(0.40,0.96)
White matter hyperintensities (WMH)							
WMH	0.630	0.188	11.25	1	0.0008	1.87	(1.30,2.71)
3MSE	−0.025	0.021	1.41	1	0.233	0.77	(0.50,1.18)
Diabetes	0.584	0.322	3.297	1	0.069	1.79	(0.95,3.37)
Global white matter fractional anisotropy (FA)							
FA	−0.291	0.111	6.84	1	0.008	0.74	(0.60,0.92)
Diabetes	−0.527	0.315	2.79	1	0.094	0.59	(0.31,1.09)
3MSE	−0.037	0.020	3.37	1	0.066	0.68	(0.45,1.02)

Psychiatry Res. Author manuscript; available in PMC 2015 November 30.